EurJIC European Journal of Inorganic Chemistry

ChemPubSoc Europe

FULL PAPER

DOI:10.1002/ejic.201500737

CLUSTER ISSUE

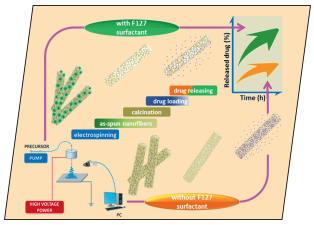

BACK COVER

Synthesis of $CaTiO_3$ Nanofibers with Controllable Drug-Release Kinetics

Qiuhong Zhang,[a] Xiang Li,*[a] Zhaohui Ren,[a] Gaorong Han,*[a] and Chuanbin Mao*[a,b]

Keywords: Sol–gel processes / Surfactants / Nanofibers / Electrospinning / Drug delivery

Calcium titanate ($CaTiO_3$) nanofibers with controlled microstructure were fabricated by a combination of sol–gel and electrospinning approaches. The fiber morphology has been found to rely significantly on the precursor composition. Altering the volume ratio of ethanol to acetic acid from 3.5 to 1.25 enables the morphology of the $CaTiO_3$ nanofibers to be transformed from fibers with a circular cross section to curved ribbon-like structures. Ibuprofen (IBU) was used as a model drug to investigate the drug-loading capacity and drug-release profile of the nanofibers. It was found that the BET surface area and the pore volume decrease markedly with the utilization of F127 surfactant. The nanofibers synthesized without F127 surfactant present the highest drug-loading capacity and the most sustained release kinetics. This study suggests that calcium titanate nanofibers can offer a promising platform for localized drug delivery.

Introduction

Research on localized drug-delivery systems (LDDSs) have received burgeoning attention and have advanced rapidly in the last years due to their great potential to improve human health. Compared with conventional forms of drug dosage, LDDSs display many advantages including greater efficacy and safety, controlled and prolonged release time, and predictable therapeutic response.[1] More recently, on the basis of the large surface area of nanofibers, the sustained drug-release kinetics, and the nontoxic nature of inorganic materials, inorganic nanofibers such as silica,[2] bioactive glass,[3] and hydroxyapatite[4] have been widely investigated as candidates for modern LDDSs.

Calcium titanate ($CaTiO_3$) is a well-known bioceramic. It has been extensively used for orthopedic implants as a coating material.[5] A $CaTiO_3$ coating layer between titanium substrate and hydroxyapatite has been demonstrated to suppress the progression of hydroxyapatite dissolution in acidic environment caused by osteoclastic bone resorption in the body.[5c,6] In addition, the growth of apatite on $CaTiO_3$ is promoted in simulated body fluids.[7] The good stability and identified biocompatibility of $CaTiO_3$ make it possible to extend its applications in localized drug delivery. To date, much effort has been devoted to the synthesis of $CaTiO_3$ micro-/nanostructures by methods such as a PEG-200-assisted solvothermal procedure,[8] the sol–gel method,[9] and hydrothermal methods.[10]

Electrospinning is a highly versatile method for preparing fibers with dimensions down to the nanometer range. Electrospun nanofibers offer several advantages such as an extremely high surface-to-volume ratio, tunable porosity, and malleability to conform to a wide variety of sizes and shapes.[11] With smaller pores and higher surface area than regular fibers, electrospun fibers have been successfully applied in diverse fields including tissue engineering,[12] biosensors,[13] filtration,[14] wound dressings,[15] drug delivery,[1a,1b,16] and enzyme immobilization.[17] The nanoscale fibers are generated by the application of a strong electric field to the polymer solution. Under a strong electric field, a jet is formed and moves towards the grounded collector. On the way to the collector, the solvent evaporates, and solid fibers with diameters ranging from micrometers to nanometers precipitate on the collector. The electrospinning technique has been utilized to synthesize dense and hollow nanofibers of inorganic ceramics such as silica,[18] bioactive glass,[3b] TiO_2,[19] SnO_2,[20] Al_2O_3,[21] In_2O_3,[22] and $CaTiO_3$.[23] Electrospinning has been proven to be a highly successful technique for controlling the synthesis of one-dimensional nanostructures.

$CaTiO_3$ nanofibers doped with rare earth elements have been synthesized by electrospinning for various optical applications.[24] However, to the best of our knowledge, there is no report on electrospun $CaTiO_3$ nanofibers for localized drug-delivery applications. Therefore, in this work we fabri-

[a] State Key Laboratory of Silicon Materials, School of Materials Science and Engineering, Zhejiang University, Hangzhou 310027, P. R. China
E-mail: xiang.li@zju.edu.cn
hgr@zju.edu.cn
[b] Department of Chemistry & Biochemistry, Stephenson Life Sciences Research Center, University of Oklahoma, 101 Stephenson Parkway, Norman, Oklahoma 73019-5300, USA
E-mail: cbmao@ou.edu

Supporting information for this article is available on the WWW under http://dx.doi.org/10.1002/ejic.201500737.

cated nanoscale $CaTiO_3$ drug carriers with a method based on the electrospinning technique with subsequent heat treatment. A surfactant-assisted sol–gel method was utilized to realize the controllable synthesis of $CaTiO_3$ nanofibers with use of Pluronic F127 as surfactant and by tuning the experimental parameters. The drug-release properties of the nanofibers were tested with ibuprofen (IBU) as a model drug.

Results and Discussion

Electrospinning Synthesis Process and Phase Structure

A schematic diagram of the electrospinning procedure of $CaTiO_3$ nanofibers is shown in Figure 1. The setup has three components: a high-voltage power supply, a metallic needle, and a grounded collector (Figure 1a). The needle is connected to a syringe in which the precursor solution is filled. With use of a syringe pump, the solution is fed through the needle at a controllable rate. When a high voltage is applied, the pendant droplet of the precursor solution at the tip of the needle becomes highly electrified, and the induced charges get evenly distributed over the surface. As a result, under the coulombic force exerted by the external electric field and the electrostatic repulsion between the surface charges, the droplet is distorted to a hemispherical object and is elongated to form a conical shape known as the Taylor cone.[25]

In our study, when the applied voltage and flow rate were set at 9.8–10.6 kV and 0.5 mL/h, respectively, a stable cone-shaped electrospinning jetting mode was achieved and maintained, as captured by a speed camera (Figure 1c). Subsequently, the jet that is highly stretched and elongated under the electric field results in the formation of continuous fine fibers owing to the blending instability.[26] When the process parameters were set outside this range, an unstable jetting mode (Figure 1b) or a multijetting mode (Figure 1d) were obtained, as a result of which non-uniform fibers were formed.

Figure 2a shows the thermogravimetric differential scanning calorimetry (TG-DSC) curves of the as-spun fibers during the calcination process by heating known quantities of fibers at a step rate of 10 °C/min in air. An increase from ambient temperature (25 °C) to 157.2 °C, which resulted in

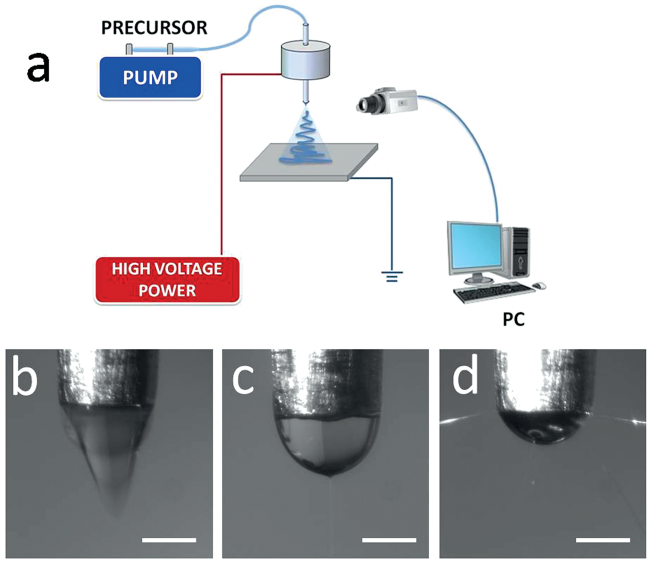

Figure 1. (a) Schematic diagram of electrospinning setup. (b–d) The high-speed camera image of the jet during electrospinning at different voltages. The scale bar is 1 mm.

about 9.89% weight loss in the TG curve, was accompanied with a weak broad endothermic peak at 74.58 °C due to the evaporation of residual solvent. Between 157.2 and 329.92 °C, about 69.61% weight loss was observed with two exothermic peaks at 219.01 and 312.66 °C, which are attributed to the decomposition of nitrates and the degradation of polyvinylpyrrolidone (PVP).[27] PVP degradation proceeds by two mechanisms involving both intramolecular and intermolecular transfer reactions.[28] Between 329.92 and 550 °C, there was about 4.31% weight loss with an exothermic peak at 463.15 °C, which is the result of oxidation of carbon and carbon monoxide released by the decomposition of tetrabutyltitanate and PVP.[27,29] No further significant weight loss was observed above 600 °C, indicating that the pyrolysis process was complete and the perovskite $CaTiO_3$ phase was formed.

Figure 2b shows X-ray diffraction (XRD) patterns of the fibers annealed at 700 °C, well-defined diffraction peaks at (110), (111), (112), (210), (103), (022), (220), (204), (224), and (110) were detected, all of which were indexed to the orthorhombic phase of $CaTiO_3$ (JCPDS No. 82–0228). No diffraction peaks from impurities were observed. This sug-

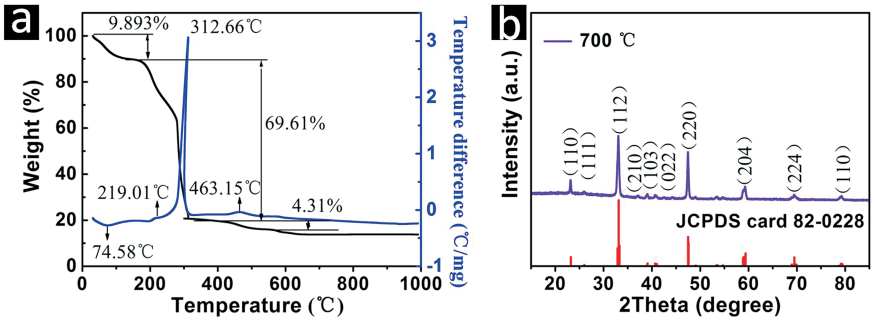

Figure 2. (a) TG-DSC curves of as-spun $CaTiO_3$ nanofibers and (b) XRD patterns of $CaTiO_3$ nanofibers annealed at 700 °C.

gests that the fibers have crystallized in the pure orthorhombic $CaTiO_3$ phase, which is in agreement with TG-DSC results.

Effect of Precursor Composition on the Fibers

In the preparation of the $CaTiO_3$ precursor sol, acetic acid retards the hydrolysis of titanium and stabilizes the sol for electrospinning. In addition, acetic acid can also absorb the moisture in the air, which decelerates the evaporation of the solvents and may induce a negative influence on the fine fiber morphology. Thus, it is of great importance to control the volume of acetic acid in the precursor solution. The influence of the ratio of ethanol to acetic acid on the fiber morphology was investigated experimentally, and sols with five different volume ratios of ethanol to acetic acid (1.25, 2, 3, 3.5, and 4) were prepared and electrospun, while keeping the other parameters constant. All the above as-spun $CaTiO_3$ nanofibers were calcined at 700 °C to eliminate PVP, surfactant, and solvent. As shown in the scanning electron microscopy (SEM) images (Figure 3), $CaTiO_3$ nanofibers obtained at different ratios presented different morphologies. When the volume ratio was set at 4, a white precipitate formed, and the precursor solution became unstable. When the ratio was set at 3 and 3.5, the nanofibers presented a mean diameter of about 106 and 114 nm, respectively, and when the ratio was less than 3, the hydrolysis of titanium butoxide was effectively hindered,[30] and the precursor was quite stable. However, curved ribbon-like $CaTiO_3$ was formed when the volume ratio of ethanol to acetic acid reached 1.25. The morphology of electrospun one-dimensional nanomaterials is dependent on a number of processing parameters including the type of polymer, electrical conductivity, surface tension, applied voltage, flow rate, nozzle-collector distance, and operational conditions.[31] Under the control of these factors, evaporation of the solvent and the subsequent collapse of the fiber might be responsible for the emergence of a ribbon-like structure.[32] Once the fiber is spun out of the nozzle during electrospinning, the solvent evaporates rapidly from the fiber, and the as-prepared fiber may completely solidify to different degrees before reaching the collector. This depends on the physical properties of the solvents. If the fibers are not completely solidified prior to reaching the collector, ribbon-like structures may form.[33]

It needs to be pointed out that acetic acid is a hygroscopic liquid with a high boiling point and ethanol is volatile at ambient temperature. When the jets are electrospun out of the nozzle, ethanol evaporates completely, while some acetic acid remains in the fiber prepared with a low volume ratio, giving rise to the formation of curved ribbon-like morphology. Thus, the volume ratio of ethanol to acetic acid plays an important role in fiber formation and structure.

The $CaTiO_3$ nanofibers synthesized with a volume ratio of 3 were further examined by using transmission electron microscopy (TEM). The microstructural characteristics of

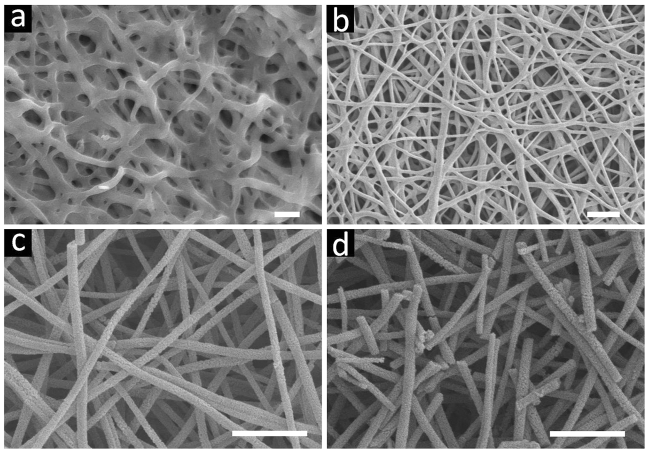

Figure 3. SEM images of $CaTiO_3$ nanofibers obtained at various volume ratios of ethanol to acetic acid: (a) 1.25, (b) 2, (c) 3, and (d) 3.5. $CaTiO_3$ nanofibers in (d) seem to be cut during the strong sonication procedure while the sample was collected prior to examination by SEM. The scale bar is 1 μm.

nanofibers when different amounts of Pluronic F127, a widely used surfactant in drug-delivery systems, were used were investigated (Figure 4). Owing to the different penetration depth of electrons in different parts of the fiber body, the highly porous nature of all fibers was clearly observed. The microstructure of nanofibers prepared with F127 surfactant shows relatively more "loosened" characteristics (Figure 4b and 4e). This indicates that the F127 surfactant induces pores with increased dimensions. In addition, the polycrystalline nature of $CaTiO_3$ nanofibers is confirmed from the selected area electron diffraction patterns (the insets of Figure 4b and 4e). The HRTEM images, shown in Figure 4c and 4f, present a large scale of neatly arranged lattice fringes with no obvious defects. The *d*-spacing values are 0.382 and 0.270 nm, corresponding to the (110) and (112) crystal facets of the orthorhombic $CaTiO_3$ phase, respectively. Those results indicate that all fibers are of fine crystallinity, which agrees well with the findings from XRD studies.

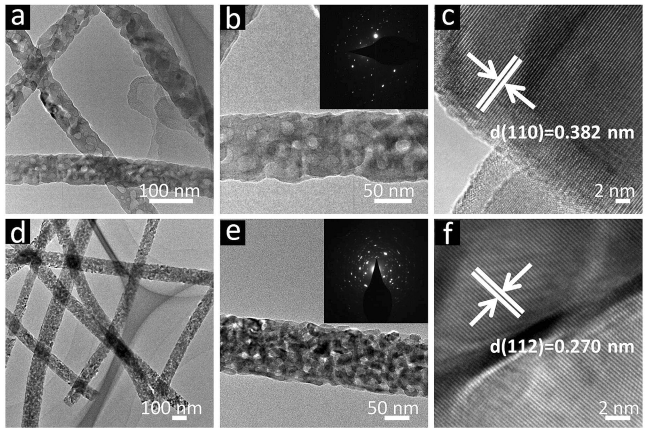

Figure 4. TEM and HRTEM images of $CaTiO_3$ nanofibers obtained with (a–c) and without (d–f) F127 surfactant. Insets: SAED pattern of a single nanofiber.

The formation mechanism of porous $CaTiO_3$ nanofibers is demonstrated in Figure 5. The precursor solution is composed of a metal salt solution, PVP, and F127 surfactant. PVP was used to adjust the viscoelastic behavior and make the sol suitable for further electrospinning. Pluronic F127 is an amphiphilic block copolymer, which has a large solubility difference between its hydrophilic and hydrophobic segments. Such copolymer molecules self-assemble into micelles, a core-shell architecture, where hydrophobic segments are segregated from the exterior solution to form an inner core surrounded by a shell of hydrophilic segments.[34] The F127 micelles can exist in the as-spun fibers. Under high-temperature sintering, $CaTiO_3$ nanofibers with porous structure are obtained, because the F127 micelle template and PVP molecules vanish. Thus, $CaTiO_3$ nanofibers prepared with or without F127 surfactant have different porous microstructures.

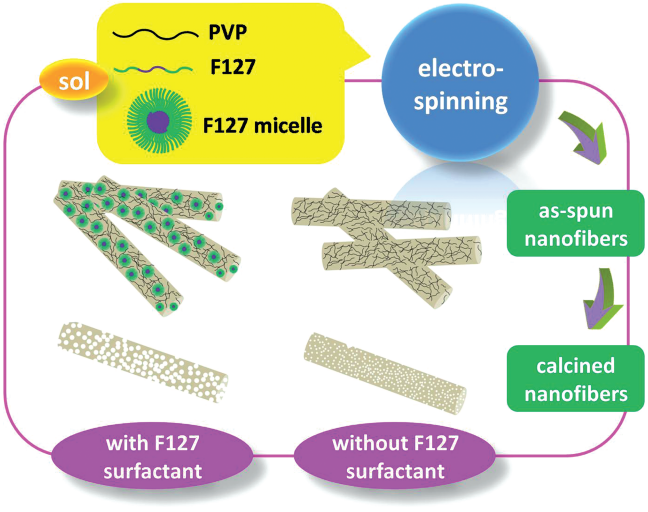

Figure 5. Illustration of the formation process of porous $CaTiO_3$ nanofibers.

The unique microstructure characteristics of $CaTiO_3$ nanofibers facilitate the potential of this material as a localized drug-delivery system. To further investigate the porosity of $CaTiO_3$ nanofibers, the specific surface area and pore characteristics of fibers were examined by using N_2 adsorption/desorption measurements. As shown in Figure 6, $CaTiO_3$ nanofibers prepared with or without F127 surfactant both showed representative IV-type isotherms, which are characteristics of typical porous materials. The specific surface area and pore volume of the fibers, calculated using the Brunauer–Emmett–Teller (BET) and Barrett–Joyner–Halenda (BJH) methods, are summarized in Table 1. The fibers synthesized with F127 have a BET surface area of about 18.1 m^2/g and a pore volume of about 0.071 cm^3/g, while those synthesized without the surfactant were found to show a higher BET surface area (ca. 30.7 m^2/g) and a larger pore volume (ca. 0.119 cm^3/g). The reason for such a difference is the formation of F127 micelles, as discussed above. This result matches those reported previously.[2a,34a,35]

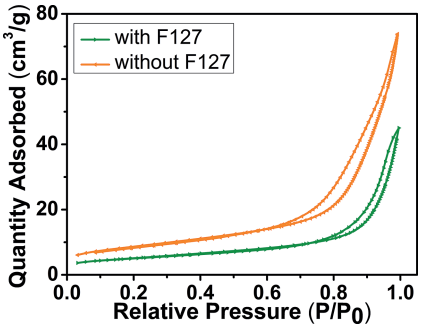

Figure 6. N_2 adsorption/desorption isotherm of $CaTiO_3$ nanofibers.

Table 1. The BET surface area, pore volume, and drug-loading capacity of $CaTiO_3$ nanofibers.

Sample	BET surface area (m^2/g)	Pore volume (cm^3/g)	Drug-loading capacity (wt.-%)
Without F127	30.7	0.119	43.7
With F127	18.1	0.071	24.5

Drug Loading and Release

Figure 7 shows the FTIR spectra of $CaTiO_3$ nanofibers, IBU-loaded $CaTiO_3$ nanofibers, and the pure IBU drug. For the $CaTiO_3$ nanofibers, strong absorption peaks at about 445 and 556 cm^{-1} are attributed to the bending mode of Ti–O.[36] The weak bands assigned to the hydroxyl absorption (3432 cm^{-1}) and the O–H vibrations of H_2O (1635 cm^{-1}) indicate the presence of hydroxyl groups and H_2O molecules on the surface of $CaTiO_3$ nanofibers, which is important for the attachment IBU molecules. When $CaTiO_3$ nanofibers were loaded with IBU molecules, typical characteristic peaks assignable to –COOH vibration at about 1720 cm^{-1} and C–H_x bonds at about 2862 and 2960 cm^{-1} were clearly observed, except for a slight decrease in intensity compared with that of pure IBU drug. Furthermore, absorption bands, which could be assigned to the quaternary carbon atom at about 1460 and 1512 cm^{-1} and to the tertiary carbon atom at 1329 cm^{-1} arising from the introduced IBU molecules, were also observed, confirming that IBU drug was successfully loaded on the $CaTiO_3$ nanofibers.

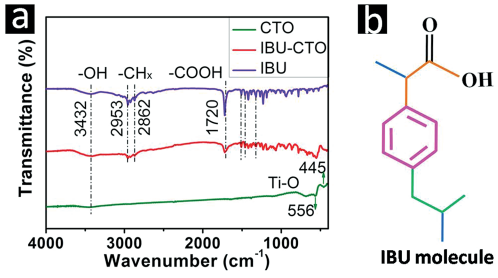

Figure 7. (a) FTIR spectra of $CaTiO_3$ nanofibers, IBU-loaded $CaTiO_3$ nanofibers, and pure IBU. (b) The molecular structure of IBU.

The absorbance of IBU in phosphate-buffered saline (PBS) solution is shown in Figure S1a. Obviously, the maxi-

mum absorbance occurs at a characteristic wavelength of 222 nm. Therefore, the in vitro examination of IBU release by UV/Vis spectroscopy was carried out at this wavelength. The relationship between absorbance at 222 nm and IBU concentration is demonstrated in Figure S1b. When the IBU concentration ranges from 0.010 to 0.025 mg/mL, the absorbance at 222 nm shows good linearity with the IBU concentration, and the correlation coefficient reaches 99.408%. The IBU concentration in the release medium can be calculated by the equation:

$$A_{222} = 31.402\ C_{IBU} + 0.1488$$

where A_{222} is the absorbance at 222 nm and C_{IBU} is the concentration of IBU in the collected sample. Hence, the drug-loading capacity and cumulative drug release can be calculated by means of the above calibration curve equation.

In the drug-loading procedure, the IBU molecules can be adsorbed onto the surface of the highly porous $CaTiO_3$ nanofibers. The drug-loading capacities of the IBU-loaded $CaTiO_3$ nanofibers prepared with and without F127 surfactant were calculated to be about 24.5 and 43.7 wt.-%, respectively. It is interesting to find that the amount of drug loaded on the fibers prepared without F127 surfactant is nearly double that loaded on the fibers prepared with surfactant. Moreover, the BET surface area and pore volume of the fibers prepared without surfactant are also nearly two times those of the fibers prepared with the surfactant, which indicates a correlation between the drug-loading capacity and the BET surface area and pore volume of the porous materials.

During the drug-release process in PBS solution, accompanied by fluid diffusion into the pores of the nanofibers, IBU molecules are liberated from the fibers and released into the fluid by a diffusion-controlled mechanism. Figure 8 shows the cumulative drug-release profiles as a function of release time for IBU-loaded $CaTiO_3$ nanofibers. Rather different release behavior was observed for the two types of $CaTiO_3$ nanofibers. A typical drug-release phenomenon consists of two stages, including an initial fast-release stage, dominated by the rapid leaching of free IBU molecules from the outer surfaces of the fibers, and a relatively slow subsequent release stage, ascribed to drug liberation from the porous structure of the fibers. The $CaTiO_3$ nanofibers synthesized without F127 surfactant present a dramatically sustained drug-release rate due to their reduced pore dimensions and increased BET surface area. About 28 wt.-% of IBU drug is liberated from the nanofibers within the initial 2 h, and about 66 wt.-% of the total IBU drug is released after 48 h. In contrast, for the $CaTiO_3$ nanofibers with low BET surface area and large pore dimensions, the amount of released IBU drug reaches about 48 and 66 wt.-% within the initial 2 and 8 h, respectively. Therefore, the drug-loading capacity and the drug-release behavior have been successfully manipulated by the synthesis of $CaTiO_3$ nanofibers with varied microstructure. Our findings suggest another promising localized drug-delivery system for a variety of pharmaceutical applications such as localized tumor therapy, which require sustained release to reduce the significant side effects of the drugs.

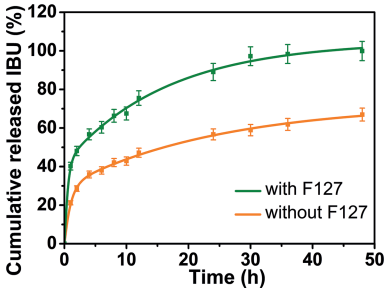

Figure 8. Cumulative drug-release profiles as a function of release time for IBU-loaded $CaTiO_3$ nanofibers.

Conclusions

A range of $CaTiO_3$ nanofibers with controlled microstructure were synthesized by a combination of the sol–gel and electrospinning methods. By tuning the volume ratio of ethanol to acetic acid, the morphology of $CaTiO_3$ nanofibers can be transformed from nanofibers with a circular cross section to ribbon-like fibers. The formation of the ribbon-like structure is ascribed to inadequate solvent evaporation from the precursor fiber before it reaches the collector. Amphiphilic block copolymer Pluronic F127 was used to vary the pore structure of $CaTiO_3$ nanofibers through self-assembly of F127 micelles and subsequent calcination. Thus the drug-loading capacity and drug-release behavior of the $CaTiO_3$ nanofibers were manipulated by altering their microstructure. As a result of their high surface area, large pore volume, and small pore dimensions, the $CaTiO_3$ nanofibers synthesized without F127 present the highest drug-loading capacity and most sustained drug-release kinetics. The study has suggested that such $CaTiO_3$ nanofibers with unique mesoporous microstructure can serve as a promising localized drug-delivery system for modern biomedical applications.

Experimental Section

Reagents and Materials: Calcium nitrate tetrahydrate [$Ca(NO_3)_2 \cdot 4H_2O$, 99%], titanium butoxide [$Ti(OC_4H_9)_4$, >98.0%], polyvinylpyrrolidone (PVP, M_W = 1,300,000, Aladdin), Pluronic F127 ($EO_{106}PO_{70}EO_{106}$, M_W = 12600, Sigma–Aldrich), Ibuprofen (IBU, 99%, Nanjing Chemical Regent Co., Ltd.), acetic acid ($C_2H_4O_2$, A.R.), ethanol (C_2H_6O, A.R.), *N*,*N*-dimethylformamide (C_3H_7NO, A.R.), and phosphate-buffered saline (PBS, pH = 7.4, Sinopharm Chemical Reagent Co., Ltd) were used as received without further purification.

Fabrication of $CaTiO_3$ Nanofibers

Briefly, $Ti(OC_4H_9)_4$ (ca. 0.82 g) and $Ca(NO_3)_2 \cdot 4H_2O$ (ca. 0.56 g) were dissolved in a mixed solution (9 mL) containing acetic acid and ethanol (volume ratio of ethanol to acetic acid 1.25, 2, 3, 3.5, and 4) with magnetic stirring. Then surfactant (Pluronic F127, 1.26 wt.-%) and polyvinylpyrrolidone (PVP, 3.25 wt.-%) were added

with *N*,*N*-dimethylformamide solution and stirred for another 6 h to form spinnable precursor sols.

The electrospinning sol was fed into the conducting nozzle (2 mm inner diameter) by using an infusion pump (KDS-100, KD Scientific, USA) at a constant flow rate of 0.5 mL/h. The distance and voltage applied between the needle tip and the collector were set at 15 cm and 10 kV (PS/FC30P04.0–22, Glassman High voltage Inc., USA), respectively. As-spun fibers were dried overnight at 80 °C and calcined in air at 700 °C for 2 h, with a heating rate of 2 °C/min.

Characterization: The thermal behavior, crystal structure, morphology, and microstructure were investigated by using TG-DSC (DSCQ1000, AT, USA, air atmosphere), XRD (X′PertPRO MPD, Netherlands, using Cu-K_α radiation, λ = 0.1540598 nm), SEM (FE SEM, Hitachi SU-70, Japan), and TEM (Philips TecnaiF20 S-TWIN, Netherlands), respectively. The specific surface area and pore size distribution were determined by N_2 adsorption/desorption analysis at liquid nitrogen temperature (77 K) by using a Coulter OMNISORP-100 apparatus. The FTIR spectra were recorded with a Perkin–Elmer 580B infrared spectrophotometer on KBr pellets (Tensor 27, Bruker, Germany). UV/Vis absorption values were measured with a TU-1810 spectrophotometer.

Drug Loading and Release

IBU-release measurements were carried out by UV/Vis absorption spectroscopy. The absorbance values were measured at a characteristic wavelength of 222 nm, at which the IBU-release medium shows the maximum absorbance. A calibration curve was drawn by plotting absorbance vs. IBU concentration.

In the drug-loading procedure, $CaTiO_3$ nanofibers (300 mg) were suspended in a hexane solution of IBU (40 mg/mL, 50 mL) at ambient temperature and stirred for 24 h to induce the diffusion of the drug into the pores. Then, the nanofibers were collected by centrifugation and washed with hexane to remove the IBU adsorbed on the outer surface. The filtrate (1 mL) was collected and diluted for the measurement of drug-loading capacity by UV/Vis spectroscopy at a wavelength of 222 nm.

In vitro drug release was investigated after IBU-loaded $CaTiO_3$ nanofibers were dried overnight at 60 °C. IBU-loaded $CaTiO_3$ nanofibers (200 mg) were immersed in the release medium PBS with gentle stirring at 37 °C. At each selected time interval, an aliquot (1 mL) was collected and immediately replaced with an equal volume of fresh PBS. The samples collected were diluted and analyzed by UV/Vis spectroscopy at a wavelength of 222 nm.

Acknowledgments

This work was financially supported by the National Nature Science Foundation of China (No. 51232006), the "Qianjiang" Talent Program of Zhejiang Province (2013R10037), and the Nature Science Foundation of Zhejiang Province (LY15E020005). C. M. would like to thank for the financial support from National Institutes of Health (EB015190) and National Science Foundation (CMMI-1234957).

[1] a) Z. Y. Hou, X. J. Li, C. X. Li, Y. L. Dai, P. A. Ma, X. Zhang, X. J. Kang, Z. Y. Cheng, J. Lin, *Langmuir* **2013**, *29*, 9473–9482; b) Y. Hong, X. Chen, X. Jing, H. Fan, B. Guo, Z. Gu, X. Zhang, *Adv. Mater.* **2010**, *22*, 754–758; c) M. Vallet-Regi, A. Ramila, R. P. del Real, J. Perez-Pariente, *Chem. Mater.* **2001**, *13*, 308–311.

[2] a) Z. Chen, X. Li, H. He, Z. Ren, Y. Liu, J. Wang, Z. Li, G. Shen, G. Han, *Colloids Surf. B* **2012**, *95*, 274–278; b) Z. Xu, S. Liu, Y. Kang, M. Wang, *Nanoscale* **2015**, *7*, 5859–5868.

[3] a) S. Huang, X. Kang, Z. Cheng, P. Ma, Y. Jia, J. Lin, *J. Colloid Interface Sci.* **2012**, *387*, 285–291; b) Y. Hong, X. Chen, X. Jing, H. Fan, Z. Gu, X. Zhang, *Adv. Funct. Mater.* **2010**, *20*, 1503–1510; c) Y. Li, B. Li, G. Xu, Z. Ahmad, Z. Ren, Y. Dong, X. Li, W. Weng, G. Han, *Colloids Surf. B* **2014**, *122*, 785–791.

[4] Z. Hou, P. Yang, H. Lian, L. Wang, C. Zhang, C. Li, R. Chai, Z. Cheng, J. Lin, *Chem. Eur. J.* **2009**, *15*, 6973–6982.

[5] a) P. Huang, K. W. Xu, Y. Han, *Mater. Lett.* **2005**, *59*, 185–189; b) H. Tang, F. Wang, *Mater. Lett.* **2013**, *93*, 427–430; c) J. P. Wiff, V. M. Fuenzalida, J. L. Arias, M. S. Fernandez, *Mater. Lett.* **2007**, *61*, 2739–2743.

[6] a) G. M. S. Kaciulis, L. Pandolfi, M. Cavalli, G. Gnappi, A. Montenero, *Appl. Surf. Sci.* **1999**, *151*, 1–5; b) S. Holliday, A. Stanishevsky, *Surf. Coat. Technol.* **2004**, *188*, 741–744.

[7] a) K. Asami, K. Saito, N. Ohtsu, S. Nagata, T. Hanawa, *Surf. Interface Anal.* **2003**, *35*, 483–488; b) T. J. Webster, C. Ergun, R. H. Doremus, W. A. Lanford, *J. Biomed. Mater. Res., Part A* **2003**, *67*, 975–980.

[8] X. F. Yang, J. X. Fu, C. J. Jin, J. A. Chen, C. L. Liang, M. M. Wu, W. Z. Zhou, *J. Am. Chem. Soc.* **2010**, *132*, 14279–14287.

[9] O. Ruzimuradov, G. Hasegawa, K. Kanamori, K. Nakanishi, *J. Am. Ceram. Soc.* **2011**, *94*, 3335–3339.

[10] D. B. Yu, J. H. Zhang, F. Wang, M. H. Zhao, K. Du, S. W. Shu, J. W. Zou, Y. Wang, *Cryst. Growth Des.* **2013**, *13*, 3138–3143.

[11] N. Bhardwaj, S. C. Kundu, *Biotechnol. Adv.* **2010**, *28*, 325–347.

[12] a) E. M. Jeffries, R. A. Allen, J. Gao, M. Pesce, Y. D. Wang, *Acta Biomaterials* **2015**, *18*, 30–39; b) C. H. Ru, F. L. Wang, M. Pang, L. N. Sun, R. H. Chen, Y. Sun, *ACS Appl. Mater. Interfaces* **2015**, *7*, 10872–10877; c) J. Thunberg, T. Kalogeropoulos, V. Kuzmenko, D. Hagg, S. Johannesson, G. Westman, P. Gatenholm, *Cellulose* **2015**, *22*, 1459–1467.

[13] a) N. Promphet, P. Rattanarat, R. Rangkupan, O. Chailapakul, N. Rodthongkum, *Sensor Actuat. B-Chem.* **2015**, *207*, 526–534; b) P. P. Zhang, X. N. Zhao, Y. C. Ji, Z. F. Ouyang, X. Wen, J. F. Li, Z. Q. Su, G. Wei, *J. Mater. Chem. B* **2015**, *3*, 2487–2496.

[14] a) Z. Wang, C. C. Zhao, Z. J. Pan, *J. Colloid Interface Sci.* **2015**, *441*, 121–129; b) X. Q. Li, N. Wang, G. Fan, J. Y. Yu, J. Gao, G. Sun, B. Ding, *J. Colloid Interface Sci.* **2015**, *439*, 12–20.

[15] a) A. Lowe, J. Bills, R. Verma, L. Lavery, K. Davis, K. J. Balkus, *Acta BioMater.* **2015**, *13*, 121–130; b) R. Zhao, X. Li, B. L. Sun, Y. Tong, Z. Q. Jiang, C. Wang, *Rsc Adv.* **2015**, *5*, 16940–16949.

[16] Z. Hou, C. Li, P. Ma, G. Li, Z. Cheng, C. Peng, D. Yang, P. Yang, J. Lin, *Adv. Funct. Mater.* **2011**, *21*, 2356–2365.

[17] a) R. Xu, Y. F. Si, F. T. Li, B. R. Zhang, *Environ. Sci. Pollut. Res. Int.* **2015**, *22*, 3838–3846; b) C. Tang, C. D. Saquing, S. W. Morton, B. N. Glatz, R. M. Kelly, S. A. Khan, *ACS Appl. Mater. Interfaces* **2014**, *6*, 11899–11906.

[18] W. Wang, J. Zhou, S. Zhang, J. Song, H. Duan, M. Zhou, C. Gong, Z. Bao, B. Lu, X. Li, W. Lan, E. Xie, *J. Mater. Chem.* **2010**, *20*, 9068.

[19] a) K. Tang, Y. Yu, X. Mu, P. A. van Aken, J. Maier, *Electrochem. Commun.* **2013**, *28*, 54–57; b) D. Li, Y. N. Xia, *Nano Lett.* **2003**, *3*, 555–560.

[20] W. Q. Li, S. Y. Ma, J. Luo, Y. Z. Mao, L. Cheng, D. J. Gengzang, X. L. Xu, S. H. Yan, *Mater. Lett.* **2014**, *132*, 338–341.

[21] P. P. Zhang, D. R. Chen, X. L. Jiao, *Eur. J. Inorg. Chem.* **2012**, 4167–4173.

[22] Z. P. Li, Y. J. Fan, J. H. Zhan, *Eur. J. Inorg. Chem.* **2010**, 3348–3353.

[23] Q. Zhang, Y. Li, Z. Ren, Z. Ahmad, X. Li, G. Han, *Mater. Lett.* **2015**, *152*, 82–85.

[24] a) C. Peng, Z. Hou, C. Zhang, G. Li, H. Lian, Z. Cheng, J. Lin, *Opt. Express* **2010**, *18*, 7543–7553; b) G. P. Dong, X. D.

Xiao, L. L. Zhang, Z. J. Ma, X. Bao, M. Y. Peng, Q. Y. Zhang, J. R. Qiu, *J. Mater. Chem.* **2011**, *21*, 2194–2203.
[25] a) A. Frenot, I. S. Chronakis, *Curr. Opin. Colloid Interface Sci.* **2003**, *8*, 64–75; b) D. H. Reneker, I. Chun, *Nanotechnology* **1996**, *7*, 216–223; c) Y. M. Shin, M. M. Hohman, M. P. Brenner, G. C. Rutledge, *Appl. Phys. Lett.* **2001**, *78*, 1149–1151; d) D. H. Reneker, A. L. Yarin, H. Fong, S. Koombhongse, *J. Appl. Phys.* **2000**, *87*, 4531–4547.
[26] a) A. L. Yarin, S. Koombhongse, D. H. Reneker, *J. Appl. Phys.* **2001**, *90*, 4836–4846; b) Y. M. Shin, M. M. Hohman, M. P. Brenner, G. C. Rutledge, *Polymer* **2001**, *42*, 9955–9967.
[27] L. L. Wang, X. M. Liu, Z. Y. Hou, C. X. Li, P. P. Yang, Z. Y. Cheng, H. Z. Lian, J. Lin, *J. Phys. Chem. C* **2008**, *112*, 18882–18888.
[28] S. J. A. M. A. Dish, *Polym. Degrad. Stab.* **1998**, *60*, 253–256.
[29] C. Peng, Z. Hou, C. Zhang, G. Li, H. Lian, Z. Cheng, J. Lin, *Opt. Express* **2010**, *18*, 7543–7553.
[30] Y. Fu, Z. Jin, Y. Ni, H. Du, T. Wang, *Thin Solid Films* **2009**, *517*, 5634–5640.
[31] A. Greiner, J. H. Wendorff, *Angew. Chem. Int. Ed.* **2007**, *46*, 5670–5703; *Angew. Chem.* **2007**, *119*, 5770.
[32] a) D. Li, Y. N. Xia, *Adv. Mater.* **2004**, *16*, 1151–1170; b) X. Guo, F. C. Szoka, *Acc. Chem. Res.* **2003**, *36*, 335–341; c) K. E. Uhrich, S. M. Cannizzaro, R. S. Langer, K. M. Shakesheff, *Chem. Rev.* **1999**, *99*, 3181–3198; d) K. Kataoka, A. Harada, Y. Nagasaki, *Adv. Drug Delivery Rev.* **2001**, *47*, 113–131.
[33] T. J. Sill, H. A. von Recum, *Biomaterials* **2008**, *29*, 1989–2006.
[34] a) J. Saha, G. De, *Chem. Commun.* **2013**, *49*, 6322–6324; b) W. Zhao, Y. L. Su, C. Li, Q. Shi, X. Ning, Z. Y. Jiang, *J. Membr. Sci.* **2008**, *318*, 405–412.
[35] a) D. Grosso, G. J. d. A. A. Soler-Illia, E. L. Crepaldi, F. Cagnol, C. Sinturel, A. Bourgeois, A. Brunet-Bruneau, H. Amenitsch, P. A. Albouy, C. m. Sanchez, *Chem. Mater.* **2003**, *15*, 4562–4570; b) P. D. Yang, D. Y. Zhao, B. F. Chmelka, G. D. Stucky, *Chem. Mater.* **1998**, *10*, 2033–2036.
[36] a) S. Maensiri, W. Nuansing, J. Klinkaewnarong, P. Laokul, J. Khemprasit, *J. Colloid Interface Sci.* **2006**, *297*, 578–583; b) H. K. Yang, J. W. Chung, G. S. R. Raju, B. K. Moon, B. C. Choi, J. H. Jeong, J. H. Kim, *Appl. Surf. Sci.* **2009**, *255*, 5062–5066; c) M. Shivaram, H. Nagabhushana, S. C. Sharma, S. C. Prashantha, B. Daruka Prasad, N. Dhananjaya, R. Hari Krishna, B. M. Nagabhushana, C. Shivakumara, R. P. Chakradhar, *Spectrochim. Acta Part A* **2014**, *128*, 891–901.
Received: July 5, 2015
Published Online: August 18, 2015

